



# Machinability Study of A286 Superalloy for Complex Profile Generation Through Wire Electric Discharge Machining

Subhankar Saha<sup>1</sup> · Saikat Ranjan Maity<sup>1</sup> · Sudip Dey<sup>1</sup>

Received: 17 February 2022 / Accepted: 5 June 2022 / Published online: 2 August 2022  
© King Fahd University of Petroleum & Minerals 2022

## Abstract

Estimation of machining time and accuracy plays a pivotal role in exemplifying the efficacy of the wire electric discharge machining (WEDM) process. The comprehensive insight on the influence of servo feed rate under different control modes (proportional control mode, constant feed mode, and constant voltage mode) on the machining time (MT), corner error (CE), and radius of the concave profile (RUC) of a convex–concave-based geometrical profile was discussed in the present research venture. Moreover, the influence of other process variables such as dielectric water pressure (WP), wire tension (WT), and servo voltage (SV) on the responses was also included in the present research. A face-centered central composite design strategy was employed to plan the experiments. The ANOVA test analyzed that SV and SF are the influential parameters for all the responses. Unlike the MT and RUC, the dielectric water pressure (WP) and wire tension (WT) were also found to influence the CE from the ANOVA analysis. Contour plots were exhibited to reveal the interaction effect between servo feed rate and servo voltage on the responses. Finally, the desirability function with the Nelder–Mead simplex algorithm was exploited to optimize the three responses simultaneously. The optimal settings determined by the proposed approach were as follows: WP = 15 kg/cm<sup>2</sup>, WT = 12 N, SV = 60 V, and SF = 2150 mm/min. FESEM micrographs and images from non-contact optical profilometry were showcased for different servo settings to demonstrate the role of servo parameters on the machined surfaces.

**Keywords** WEDM · Control modes · Desirability function · Nelder–Mead simplex algorithm · FESEM

## 1 Introduction

Wire electric discharge machining (WEDM) process has gained immense popularity in many high-added-value sectors such as aerospace, automobile, medical, and nuclear due to its potential to produce complex-shaped cuts. A succession of discrete spark discharges between a continually moving wire and the workpiece of electrically conductive material melts and evaporates the work material. Later, jets of dielectric fluid are delivered into the space between the wire-work-piece combinations to expel the melted waste.

Because of the contactless machining, hardness and other mechanical properties of any material do not impose any practical constraints on this machining process, making it superior to conventional machining approaches. In WEDM, high accurate parts are achieved except in the case of a corner and small-radius arcs where accuracy is lost due to the wire lag phenomena. Many research investigations have been reported in the literature to deal with this problem of wire lag and its adverse effects. Dekeyser and Snoeys [1] proposed an off-line path modification technique to improve profile accuracy. Exploiting an online optical wire position sensor, Dauw et al. [2] created an online wire path control system. Hsue et al. [3] investigated the unstable phenomena of machining parameters at the corner. Lin et al. [4] proposed a fuzzy control technique to increase corner accuracy by increasing the pulse off time. Puri and Bhattacharyya [5] used the Taguchi approach to reduce corner error in trim cutting operations by optimizing process parameters. Sarkar et al. [6] proposed a wire lag prediction model based on the gap force intensity concept. Selvakumar et al. [7, 8] used a parameter

✉ Saikat Ranjan Maity  
saikat.jumtech@gmail.com

Subhankar Saha  
sahamech90@gmail.com

Sudip Dey  
infodrsudip@gmail.com

<sup>1</sup> Department of Mechanical Engineering, National Institute of Technology Silchar, Silchar, Assam, India



modification strategy and trim cutting operation to investigate the WEDM corner accuracy of the Monel 400 alloy. Kumar et al. [9] discovered that pulse on time, pulse off time, and spark voltage substantially impact dimensional variation. Sonawane et al. [10] also stated the significant impact of similar parameters on overcut. Firouzabadi et al. [11] studied the geometrical inaccuracy of corners. According to their findings, controlling process parameters may reduce errors, but it is unlikely to abolish them completely. In another investigation, improvement in corner accuracy is achieved by devising an online closed-loop wire tension control system [12]. Sanchez et al. [13] proposed a computer-integrated system to allow the user to choose either the wire path modification strategy or cutting regime modification depending on the requirement. Another research group emphasized the effect of multiple finish cuts and the cutting speed limitations on corner accuracy [14]. Werner et al. [15] established a strategy to enhance the accuracy of the curvilinear profile. Conde et al. [16] concluded that wire lag affects circles with less than a 3 mm radius. Chen et al. [17] used mathematical modeling to investigate wire deflection and its impact on corner accuracy during wire EDM rough machining of Ti6Al4V titanium alloy. A cut-back approach is presented based on the wire deflection model to compensate wire electrode path and increase accuracy during rough corner-cutting in WEDM. In another research, efforts are made to carry out optimization with the intent to diminish corner inaccuracies for three sets of angular cuts during rough cutting. An elliptical fitting approach is proposed to define the wire trajectory, and a Taguchi optimization method is proposed to optimize the parameters for improved accuracy [18]. Abyar et al. [19] propose a novel mathematical methodology to analyze the wire deflection in small arced corners in the WEDM process. The contribution of important parameters such as discharge frequency and wire tension is also included in the model. Another group adopted the surface feed in the wire lag model of Abyar et al. [19] to demonstrate the influence of constant feed mode on wire lag. This new model has been implemented in a program that converts G-code for machining to compensate for wire lag at sharp corners [20]. Chakraborty et al. [21] exploited a parameter modification strategy to minimize the corner inaccuracy of Inconel 718 alloy in the WEDM process. Bisaria et al. [22] investigated the effect of spark on time, wire tension, spark off time, servo voltage, and wire feed rate on corner error formed on Ni50.89Ti 49.11 shape memory alloy with 60°, 90°, and 120° triangular profiles. Naveed et al. [23] optimized geometrical accuracy for concave and convex curved profiles in WC–Co machining. Using optimal WEDM parameter settings, they discovered that both types of profiles could be machined to a 10 µm tolerance. Selvakumar et al. [24] researched the effect of multiple cuts on the WEDM of AA5083 alloy. Yan et al. [25] investigated the effect of process variables such as pulse

on time (Ton), pulse off time (Toff), magnetic field strength (B), and pulse peak current (Ip) on the corner accuracy of a thin-walled Q235 steel form component in WEDM. Mandal et al. [26] researched corner accuracy for WEDM of Al 7075 alloy. The corner accuracy is more influenced by pulse on time, servo voltage, pulse off time, and flushing pressure. The concise literature review discussed the efforts put forth by different research groups in undermining the geometrical inaccuracy with wire path modification strategy, parameter modification strategy, and using trim cuts.

Servo control strategies play a vital role in determining the machining rate and accuracy of complicated profiles due to their influence on spark frequency and the resulted wire vibration and wire deflection. The comprehensive investigation of the effect of servo feed rate under varying control modes on the geometrical accuracy of complicated profiles remains unexplored. To this end, we aimed to investigate the impact of servo feed rate under different control modes on three vital machining performances such as the machining time (MT), radius of the concave profile due to undercutting (RUC), and the corner error (CE). The different control modes are proportional control mode, constant feeding mode, and constant voltage mode. We also attempt to scrutinize the interplay between servo voltage (SV) and servo feed rate on the considered responses with the help of contour plots. The effect of mechanical parameters such as the dielectric water pressure (WP) and wire tension (WT), on the performance attributes, is also included in this investigation. Although, we have investigated the WEDM of the work material (A286 superalloy) to assess the different aspects of machining with a simple geometry in the preceding research [27]. However, an investigation of the kind emphasized in the present paper is not reported for the similar material. The present paper also proposes integrating the desirability function and Nelder–Mead simplex algorithm to optimize MT, RUC, and CE simultaneously. The optimization steps are expounded with the help of a flowchart (Fig. 1). Finally, FESEM and non-contact optical profilometer are used to retrieve information on the typical features and topography of the machined surfaces at varying servo settings.

## 2 Materials and Methods

The material considered for the present work is the A286 Superalloy. This material is chemically composed of Co (0.070 wt %), V (0.340 wt %), Ti (2.21 wt %), Cu (0.090 wt %), Al (0.16 wt %), Mo (1.23 wt %), Ni (24.57 wt %), Cr (14.7 wt %), S (0.001 wt %), P (0.013 wt %), Mn (0.250 wt %), Si (0.180 wt %), C (0.040 wt %) and Fe (Balance). A286 Superalloy is widely exploited in the gas turbine industry due to its superior mechanical properties and good thermal resistance. This material also finds applications in many areas

**Fig. 1** Flowchart illustrating steps of optimization

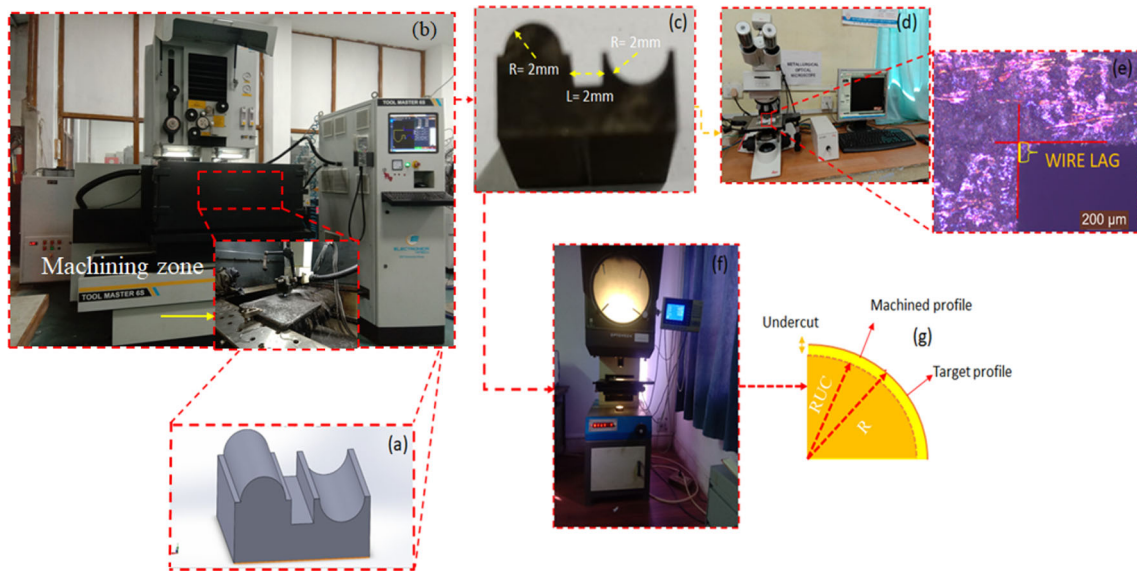
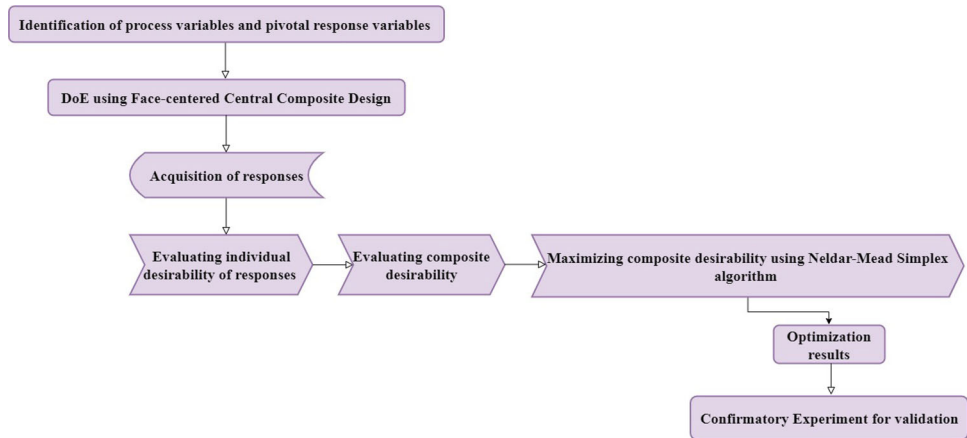


**Fig. 2** a CAD model b wire EDM machine c machined specimen d optical microscope e wire lag f vertical profile projector g undercut

**Table 1** Specification and accuracy of machine tool

Specifications		
Longitudinal travel	X	600 mm
	V	± 60
Lateral	Y	400 mm
	U	± 60
Vertical travel	Z	360 mm
Table size	875 × 595 mm	
Accuracy	0.01 mm	

such as cryogenic devices and nuclear industry. [28, 29]. In the present investigation, we conducted a machining operation on the Tool Master 6S Wire EDM machine, as shown in Fig. 2(b). The specification and accuracy of the machine tool are tabulated below (Table 1):

In the WEDM machine, there was a provision for machining under two modes, i.e., submerged mode and flushing mode, we utilized the flushing mode for the machining operations. Zinc-coated brass wire of 0.25 mm diameter was engaged as the tool electrode as it promotes sound conditions in the spark gap. Four parameters, such as the dielectric water pressure (WP), wire tension (WT), servo voltage (SV), and servo feed rate (SF), were tuned while machining. For servo feed rate (SF), the three levels were confiscated from the three control modes (shown in Table 2). The control modes are stated in brief as below:

**Proportional control mode:** In this mode, the cutting speed ( $V_c$ ) is proportional to the error voltage, where the error voltage is the difference between the actual gap voltage ( $V_g$ ) and the reference input voltage ( $V_r$ ). Thus,  $(V_c) = K (V_g - V_r)$ , where K reveals the proportional controller gain.

**Table 2** Process parameters and levels

Process parameters	Levels		
	Level 1	Level 2	Level 3
WP (kg/cm <sup>2</sup> )	7	11	15
WT (N)	6	9	12
SV (volt)	30	45	60
SF (mm/min)	120 (proportional control mode)	1135 (constant feed mode)	2150 (constant voltage mode)

**Table 3** Fixed parameters and levels

Parameters	Corresponding value
Pulse duration time ( $P_{on}$ )	115 $\mu$ s
Pulse width interval ( $P_{off}$ )	55 $\mu$ s
Peak current ( $I_p$ )	12 A
Pulse peak voltage (VP)	1 machine unit
Wire feed rate (Wf)	4 m/min
Corner dwell (CDL)	2 s
Corner control (CC %)	5
Set conductivity (S)	20 $\mu$ si/cm
Cutting speed override (CS %)	100 machine unit

**Constant feed mode:** In this mode, the cutting speed is unaffected by the gap voltage, and the wire travels at a constant speed through the workpiece which is often referred to as “blind feeding”.

**Constant voltage mode:** The gap voltage remains practically constant when this control action is used.

The three levels of the other parameters (as shown in Table 2) were chosen based on a few trial experiments. The parameters which were decided to remain untuned are revealed in Table 3. With the levels decided, we intended to use the face-centered, central composite design among the available designs in RSM to plan the experiments. This design proposes 30 experimental runs inclusive of 16 cube points, 8 axial points, 4 center points in cube, and 2 center points in axial. The CAD model of the geometry proposed for this experimental investigation is shown in Fig. 2(a). Three performance attributes, i.e., machining time (MT), radius of the concave profile due to undercutting (RUC), and corner error (CE) were assessed from the experimental expedition (revealed in Table 4). The specimen acquired after the machining is portrayed in Fig. 2(c). Optical microscope and vertical profile projector (shown in Fig. 2(d) and (f)) were employed to assess the geometrical parameters. For the sake of brevity, we have excluded the radius of convex profile formed due to overcutting in the present analysis.

## 3 Results and Discussion

### 3.1 RSM models and Statistical Analysis

The mathematical correlation between the performance and explanatory variables succeeded by statistical analyses is performed in the Design Expert 13 version. The quadratic model excluding two terms, i.e.,  $A^2$  and  $B^2$  for MT, full quadratic model for RUC, and linear + interaction terms for CE is recommended. To check whether the fundamental assumptions hold good for all these models, diagnostic plots such as the normality probability plot and residual vs. predicted plots are furnished, as revealed in Fig. 3. As noticed in Fig. 3(a), (c), and (e), the data points are well distributed along the straight line and symmetric, which corroborates that the normality assumption is satisfied for all the prescribed models. Furthermore, the externally studentized residuals for the models (shown in Fig. 3(b), (d), and (f)) appear to be randomly distributed with no systematic, funnel-shaped pattern that meets the constant variance requirement. The quality of fit and generalization prowess of the models are displayed using the scatter plots and fit statistics. The scatter plots in Fig. 4(a), (b), and (c), which correspond to MT, RUC, and CE, indicate that the goodness of fits is satisfactory for all the models. The fit statistics for the regression models for MT, RUC, and CE are delineated in Table 5. It is noticed that for all the models, the predicted  $R^2$  reasonably endorses with the Adjusted  $R^2$  as the variation between them is less than 0.2. Adequate precision, which portrays the signal-to-noise ratio, must have a ratio of more than four. The signal-to-noise ratio of 30.050, 25.269, and 52.620 for MT, RUC, and CE models suggests a good signal. Therefore, the design space can be navigated using these models.

An ANOVA test is conducted for the performance attributes to comprehend the significant process variables and other terms. Table 6 presents the ANOVA test for MT. It is noted that SV and SF are the most influencing process parameters as p values for these parameters are extremely low, i.e., much lesser than 0.05. Whereas ANOVA test for RUC, as shown in Table 7, confirms three process parameters, i.e., SV, SF, and WP, significantly influence RUC since p values for these parameters are less than 0.05. Table 8 depicts that all the process parameters, i.e., WP, WT, SV, and SF, tend to influence the response CE significantly as p values for these parameters are found to be less than 0.05.

### 3.2 Effect of Process Parameters on MT, RUC, and CE

The interaction between servo voltage and servo feed rate is prominent in the ANOVA analysis for all three performance parameters. To this end, the contour plots that depict the interaction between these parameters have only been included in this discussion. High servo feed rates enable the wire

**Table 4** Experimental runs

Run	Space type	A:WP	B:WT	C:SV	D:SF	MT (min)	RUC (μm)	CE (μm)
1	Axial	15	9	45	1135	24.57	1.95	155.95
2	Center	11	9	45	1135	24.38	1.955	155.9
3	Center	11	9	45	1135	24.39	1.956	154.55
4	Factorial	15	12	30	120	28	1.935	165.7
5	Factorial	7	6	60	2150	37.5	1.966	111.37
6	Factorial	7	6	30	2150	26.51	1.92	190.57
7	Factorial	7	12	30	2150	26	1.925	187.85
8	Axial	11	12	45	1135	23.3	1.951	153.3
9	Factorial	7	6	60	120	49	1.964	145.5
10	Center	11	9	45	1135	24.36	1.957	154
11	Center	11	9	45	1135	24.42	1.956	155.5
12	Factorial	15	6	30	120	25	1.925	170.43
13	Factorial	7	6	30	120	27	1.94	160.5
14	Axial	11	9	60	1135	30.37	1.964	126.69
15	Center	11	9	45	1135	24.4	1.955	155
16	Axial	11	6	45	1135	24.4	1.954	154.45
17	Factorial	15	6	60	2150	35.16	1.967	116.88
18	Axial	11	9	45	120	33.25	1.962	152.65
19	Factorial	7	12	60	2150	31.5	1.965	108.71
20	Center	11	9	45	1135	24.37	1.957	155.75
21	Factorial	15	12	30	2150	22.28	1.927	189.7
22	Factorial	15	6	30	2150	22.58	1.928	191.254
23	Factorial	7	12	60	120	50.11	1.967	142.8
24	Factorial	7	12	30	120	28.07	1.93	157.83
25	Axial	7	9	45	1135	23.36	1.958	155.21
26	Factorial	15	12	60	120	48	1.967	144.56
27	Axial	11	9	45	2150	28	1.948	157
28	Axial	11	9	30	1135	21.24	1.929	182.5
29	Factorial	15	6	60	120	48.19	1.965	147.7
30	Factorial	15	12	60	2150	32.36	1.97	110.5

**Table 5** Fit statistics

Models	MT	RUC	CE
$R^2$	0.9847	0.9750	0.9910
Adjusted $R^2$	0.9704	0.9690	0.9862
Predicted $R^2$	0.9092	0.9288	0.9675

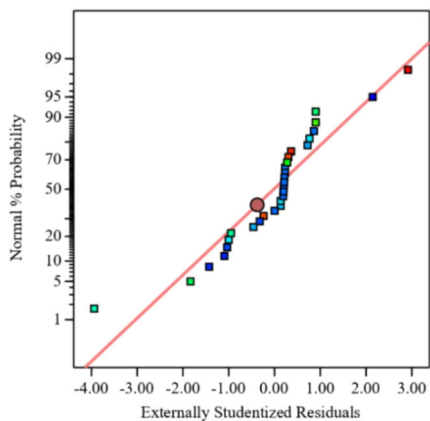
to remain closer to the workpiece at the low servo voltage settings, i.e., at 30–35 V, thereby complying with the predefined servo voltage control, exposing the wire to more severe sparks and resulting in shortened machining time, as illustrated in Fig. 5. However, it is noted that with the increment in the servo voltage settings, the servo feed rates in the continuous feeding mode conceded the wire to maintain the minimal possible distance with the workpiece, resulting in the shortest

machining time. However, the interplay between servo voltage at higher settings and servo feed rates in the proportional mode (0–1000) has the synergistic effect of increasing the wire–workpiece distance and instability in the wire position resulting in fewer severed sparks and slightly higher machining time. The same trend of increased machining time can be discerned when the servo feed rates are in the domain of constant voltage mode (2000–2150) at higher servo voltage settings.

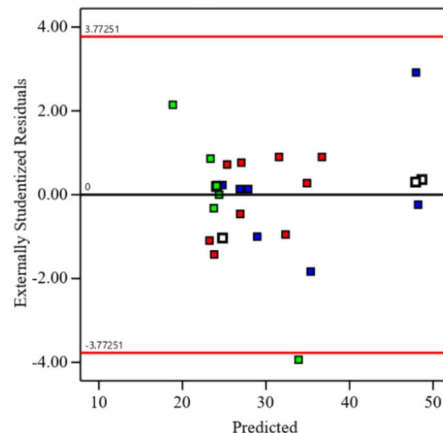
Undercuts and corner errors are quintessential features during WEDM of complicated profiles. The undercut in the concave profile leads to pruning of the actual radius of the concave profile. Whereas corner error represents the deviation of the machined corner from the actual corner. In the present article, RUC represents the radius of the concave profile due to undercutting (revealed in Fig. 2(g)), and CE



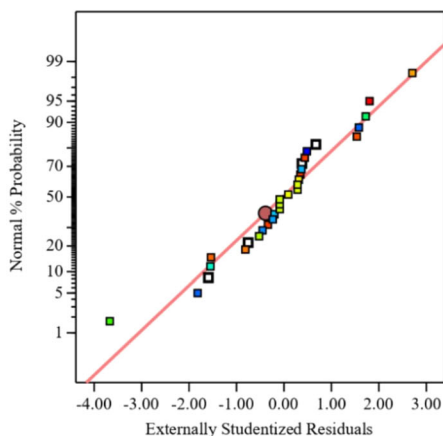
**Fig. 3** a, c, and e indicates normality plots of MT, RUC, and CE, respectively, b, d, and f indicates residual plots of MT, RUC, and CE, respectively



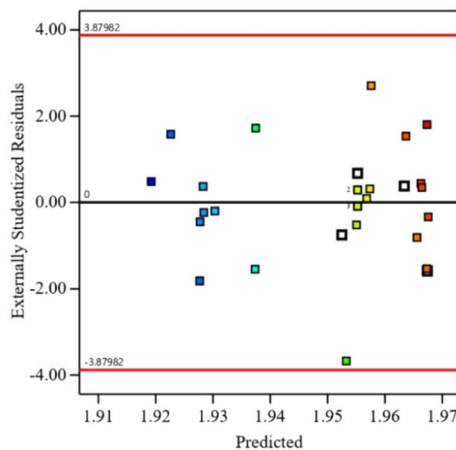
(a)



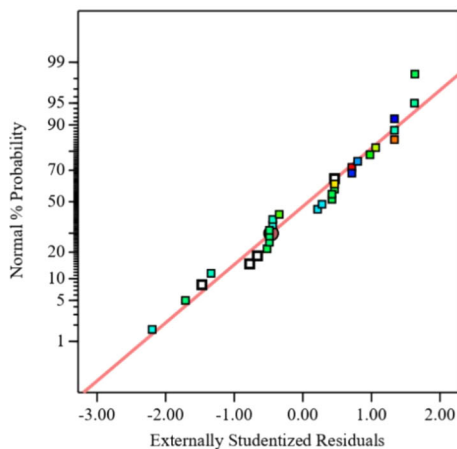
(b)



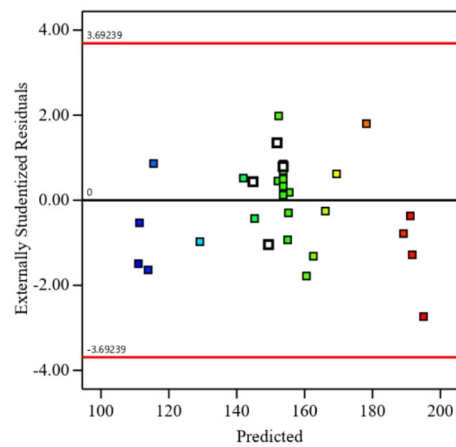
(c)



(d)



(e)



(f)

**Fig. 4** Scatter plots **a** MT, **b** RUC, and **c** CE

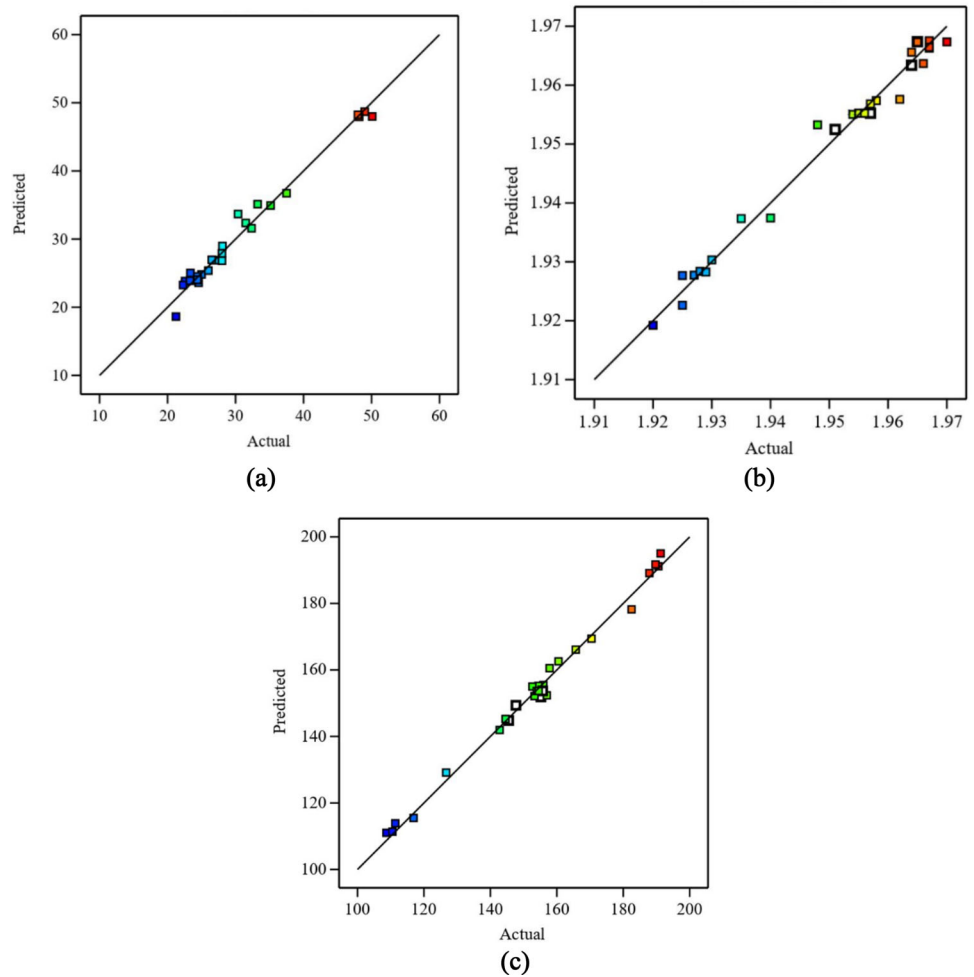


**Table 6** ANOVA test for MT

Source	Sum of squares	df	Mean square	F-value	p value
Model	2085.14	12	173.76	76.48	< 0.0001
A-WP	9.26	1	9.26	4.08	0.0596
B-WT	1.82	1	1.82	0.8000	0.3836
C-SV	1020.16	1	1020.16	449.00	< 0.0001
D-SF	310.25	1	310.25	136.55	< 0.0001
AB	1.02	1	1.02	0.4490	0.5118
AC	1.77	1	1.77	0.7785	0.3899
AD	1.07	1	1.07	0.4715	0.5016
BC	7.76	1	7.76	3.41	0.0821
BD	13.32	1	13.32	5.86	0.0269
CD	144.48	1	144.48	63.59	< 0.0001
C <sup>2</sup>	18.28	1	18.28	8.04	0.0114
D <sup>2</sup>	174.79	1	174.79	76.93	< 0.0001
Residual	38.63	17	2.27		
Lack of Fit	38.62	12	3.22	6897.03	< 0.0001
Pure Error	0.0023	5	0.0005		
Cor Total	2123.77	29			

**Table 7** ANOVA test for RUC

Source	Sum of squares	df	Mean Square	F-value	<i>p</i> value	
Model	0.0069	14	0.0005	31.96	< 0.0001	Significant
A-WP	5.556E-08	1	5.556E-08	0.0036	0.9530	
B-WT	3.556E-06	1	3.556E-06	0.2304	0.6382	
C-SV	0.0063	1	0.0063	406.38	< 0.0001	
D-SF	0.0001	1	0.0001	5.48	0.0335	
AB	0.0000	1	0.0000	1.17	0.2964	
AC	3.063E-06	1	3.063E-06	0.1984	0.6624	
AD	0.0000	1	0.0000	2.53	0.1325	
BC	5.625E-07	1	5.625E-07	0.0364	0.8512	
BD	6.250E-08	1	6.250E-08	0.0040	0.9501	
CD	0.0001	1	0.0001	4.96	0.0417	
A <sup>2</sup>	3.907E-08	1	3.907E-08	0.0025	0.9605	
B <sup>2</sup>	4.914E-06	1	4.914E-06	0.3184	0.5809	
C <sup>2</sup>	0.0001	1	0.0001	9.14	0.0086	
D <sup>2</sup>	3.266E-06	1	3.266E-06	0.2116	0.6521	
Residual	0.0002	15	0.0000			
Lack of fit	0.0002	10	0.0000	28.44	0.0009	Significant
Pure error	4.000E-06	5	8.000E-07			
Cor total	0.0071	29				

**Table 8** ANOVA test for CE

Source	Sum of squares	df	Mean square	F-value	<i>p</i> value	
Model	14,524.33	10	1452.43	208.96	< 0.0001	Significant
A-WP	58.08	1	58.08	8.36	0.0094	
B-WT	42.64	1	42.64	6.13	0.0228	
C-SV	10,835.10	1	10,835.10	1558.83	< 0.0001	
D-SF	31.56	1	31.56	4.54	0.0464	
AB	1.60	1	1.60	0.2297	0.6372	
AC	5.15	1	5.15	0.7404	0.4003	
AD	8.89	1	8.89	1.28	0.2722	
BC	0.6424	1	0.6424	0.0924	0.7644	
BD	0.0003	1	0.0003	0.0000	0.9945	
CD	3540.67	1	3540.67	509.39	< 0.0001	
Residual	132.06	19	6.95			
Lack of fit	129.32	14	9.24	16.84	0.0028	Significant
Pure error	2.74	5	0.5487			
Cor total	14,656.39	29				

represents the corner error. In the present paper, wire lag provides an estimation of CE (shown in Fig. 2(e)).

Lower RUC is acquired at servo voltages in 30–45 due to severe undercutting, as shown in Fig. 6. Because of the lesser servo voltages, the wire is compelled to be exposed to highly intensified sparks ensuing substantial deflection of the wire from its programmed path contributing to immoderate undercutting. At lower servo voltage settings, it is noted that

the high servo feed rates, i.e., constant feeding mode and constant voltage mode (range of 1000–2150) enable the wire to remain in contiguity with the workpiece leading to conserve the normal sparking rate and thus promoting undercutting. With increasing the servo voltage, i.e., in the band of 55–60, as the gap between the wire and the workpiece widens, the spark intensity drops, leading to less deflection of the wire and promoting the convergence of RUC with the radius of the



actual profile. Furthermore, even with increasing the servo feed rates, there is no evidence of augmenting the undercuts as the vibration amplitude of the wire is higher relative to the forward motion of the wire. Figure 7 reveals the contour plot representing the variation of corner error as the function of servo voltage and servo feed rate. As noticed in RUC, the same trend holds good, i.e., with the shift of servo feed rates from its proportional mode of control (0–1000) to constant voltage mode control (2000–2150) at lower voltage settings, the corner error increases. However, the servo feed rates have the least effect in the interim range of servo voltage settings (40–55). Whereas at higher servo voltage settings, raising the servo feed rates triggers a reverse effect, i.e., the CE diminishes. This is attributed to the to and fro motion of the wire due to ambiguity created by the interaction between servo voltage and servo feed rates. As a result, the wire remains unsteady near the workpiece, which leads to curtailment of the normal sparking rate.

#### 4 Multiple Performance Optimization Using Desirability Function Integrated with Nelder–Mead Simplex Algorithm

When the optimization procedure involves multiple responses, it is futile to optimize a single response separately. To put it another way, we must undergo optimization of the responses simultaneously to reach a compromise solution. In the present paper, three responses, such as MT, RUC, and CE, are optimized simultaneously. To this end, we intend to use the integrated framework, i.e., desirability function with the Nelder–Mead simplex algorithm.

As proposed by Derringer and Suich [30–32], the desirability function approach is the most elegant technique to optimize multiple responses simultaneously. It commences with transforming each response into its desirability function ( $d_i$ ) value. The desirability function ( $d_i$ ) takes values ranging from 0 to 1. If the response is the most desired, its desirability function value is 1. Whereas if the response is the most undesired value, its desirability function value is 0. Intermediate function values imply mediocre responses. Varying functional forms are exploited to calculate the desirability function values of responses. These functions depend on the optimization criteria, i.e., either Lower-the-better (LB) or Higher-the-better (HB). The desirability functions for the Lower-the-better criterion are illustrated below:

$$\text{If } \tilde{R} \leq R_{\min}, d_i = 1 \tag{1}$$

$$\text{If } R_{\min} \leq \tilde{R} \leq R_{\max}, d_i = \left[ \frac{\tilde{R} - R_{\max}}{R_{\min} - R_{\max}} \right]^p \tag{2}$$

$$\text{If } \tilde{R} \geq R_{\max}, d_i = 0 \tag{3}$$

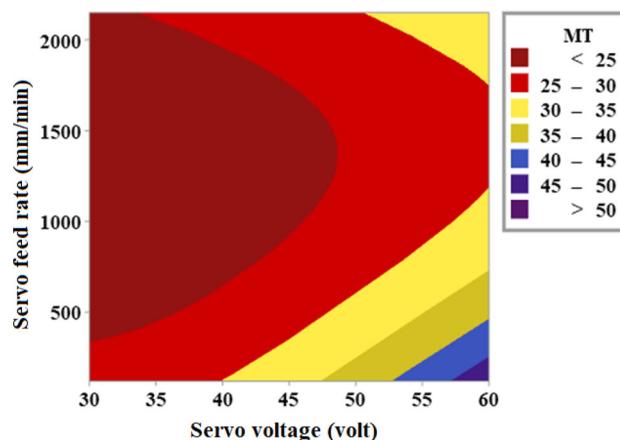


Fig. 5 Contour plot revealing interaction effect of servo voltage and servo feed rate on MT

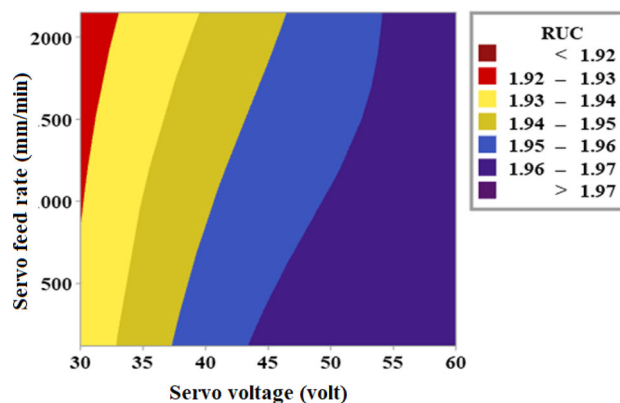


Fig. 6 Contour plot revealing interaction effect of servo voltage and servo feed rate on RUC

where as the desirability functions for the Higher-the-better criterion are illustrated below:

$$\text{If } \tilde{R} \leq R_{\min}, d_i = 0 \tag{4}$$

$$\text{If } R_{\min} \leq \tilde{R} \leq R_{\max}, d_i = \left[ \frac{\tilde{R} - R_{\min}}{R_{\max} - R_{\min}} \right]^p \tag{5}$$

$$\text{If } \tilde{R} \geq R_{\max}, d_i = 1 \tag{6}$$

$\tilde{R}$  depicts the response, whereas  $R_{\min}$  and  $R_{\max}$  depict the lower and upper bound of  $\tilde{R}$ , respectively. The value of  $p$  is user-specified, and it is assigned as 1 (linear discriminant function). Ensuing the evaluation of the individual desirability value for the multiple responses, the next step is to amalgamate the individual desirability of the responses into

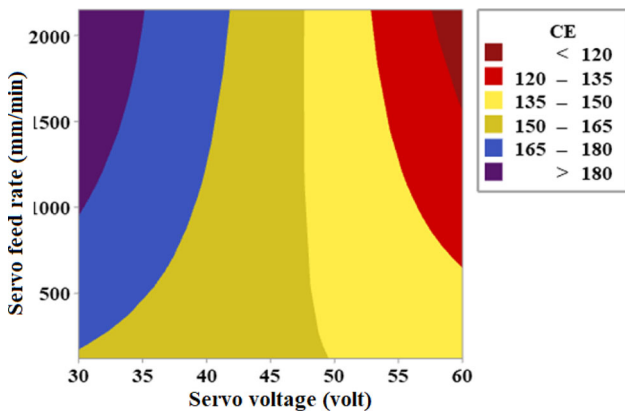


**Fig. 7** Contour plot revealing interaction effect of servo voltage and servo feed rate on CE

a composite desirability ( $D_c$ ) using geometric mean as portrayed below:

$$D_c = (d_1^{W_1} \times d_2^{W_2} \dots d_n^{W_n})^{\frac{1}{\sum W_i}} = \left( \prod_{i=1}^n d_i^{W_i} \right)^{\frac{1}{\sum W_i}} \quad (7)$$

where  $W_i$  represents the relative priority of each response over the other responses.

Nelder–Mead simplex algorithm provides a direct search strategy that can handle discontinuous functions such as desirability. The Nelder–Mead algorithm is based on improving a simplex over time. A comparison of the individual

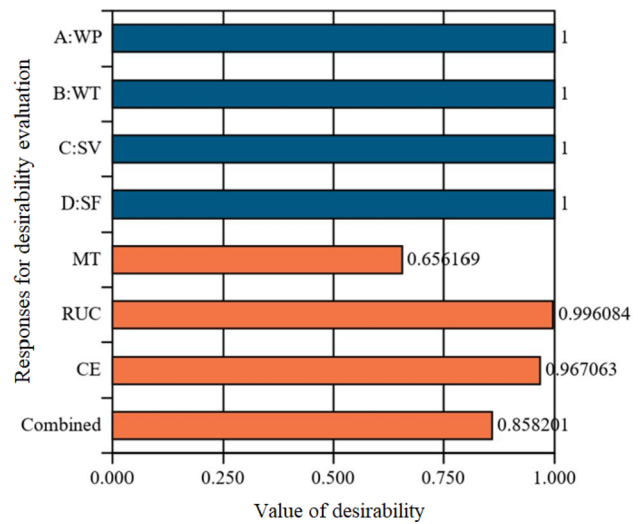


**Fig. 9** Bar plots revealing the desirability of MT, RUC, and CE and the combined desirability

function values, which stretch the simplex, is used to achieve the improvement. The worst point is to be replaced by a better one so that a simplex emerges once more [33, 34].

In the present investigation, the steps executed to carry out the optimization process are demonstrated as follows: First, we evaluated the individual desirability of the response variables using Eqs. (1, 2, 3, 4, 5, 6). To this end, we have set the goals of the responses such as for MT and CE; we set the goal as Lower-the-better (LB). On the contrary, we have set the

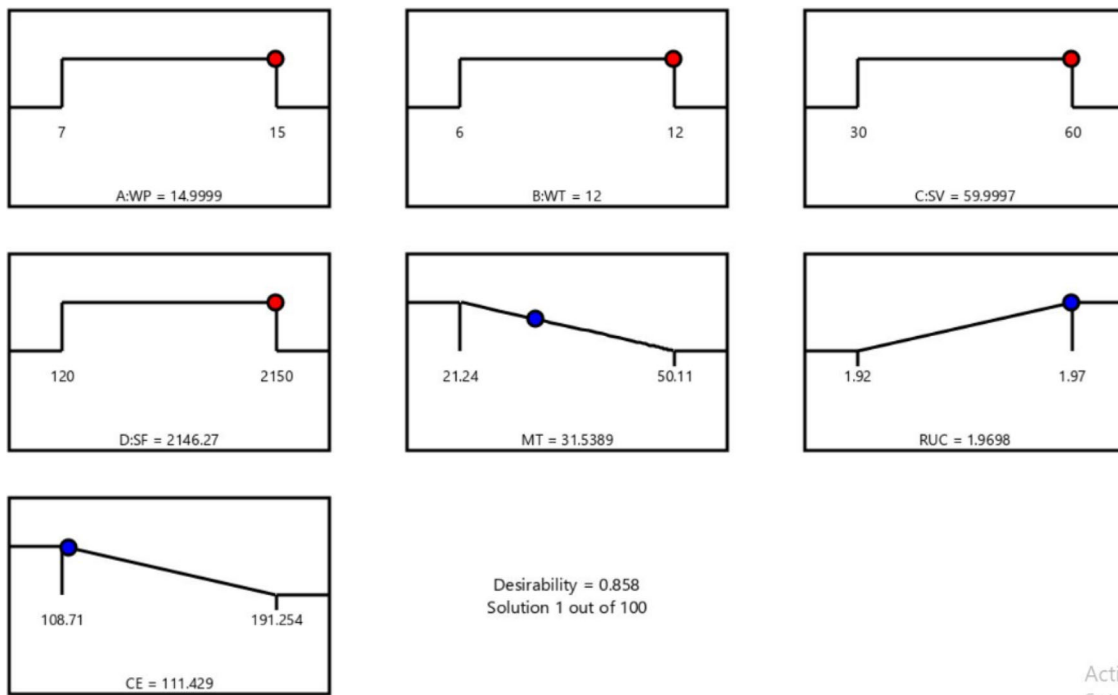
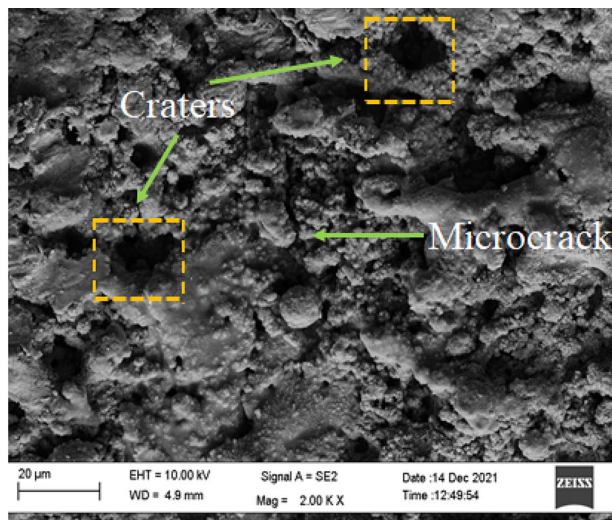
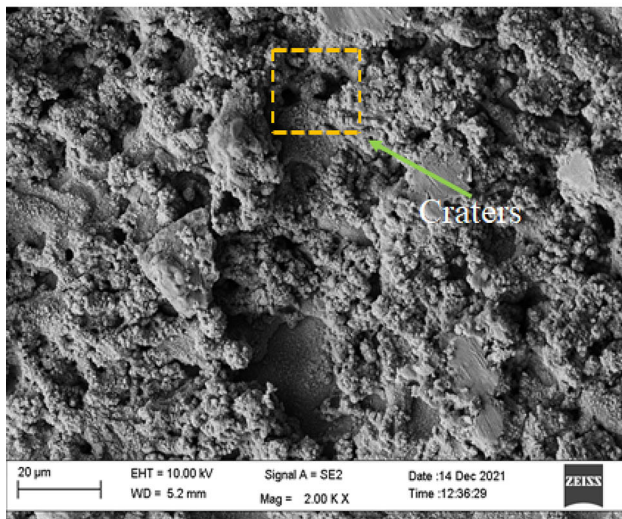


**Fig. 8** Ramp function graphs revealing the optimal factor settings and the optimal responses



(a)



(b)

**Fig. 10** FESEM micrographs **a** SV = 30 V, SF = 2150 mm/min, **b** SV = 60 V, SF = 2150 mm/min

goal for RUC as Higher-the-better (HB). While calculating the desirability function values, the lower and upper bound of the responses is attained in Table 3. Ensuing the estimation of individual desirability for all the responses, we estimated the composite desirability using Eq. (7). We have set equal priority for all the responses in the present investigation. To achieve the optimal process parametric state, the composite desirability ( $D_c$ ) is maximized using the Nelder–Mead simplex algorithm.

The ramps portrayed in Fig. 8 exhibit the optimal factor settings ( $WP = 15 \text{ kg/cm}^2$ ,  $WT = 12 \text{ N}$ ,  $SV = 60 \text{ V}$ , and  $SF = 2150 \text{ mm/min}$ ) and the optimal responses ( $MT = 31.54 \text{ min}$ ,  $RUC = 1.97 \text{ μm}$ , and  $CE = 111.43 \text{ μm}$ ) derived using the combined strategy. The red dots represent

the optimal factor settings, whereas the blue dots represent the optimal responses. Bar graphs revealed in Fig. 9 expose the individual desirability achieved by the responses and the combined desirability of 0.858, which is close to 1. The predicted optimal responses are found to be in parity with the experimental number 30.

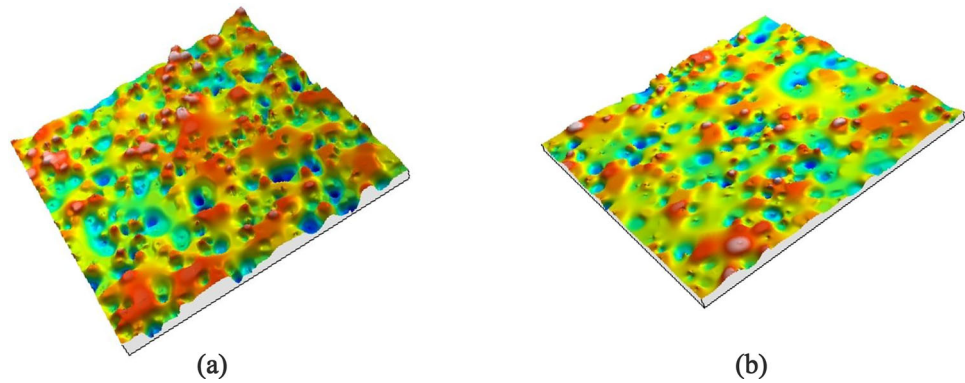
## 5.5. Surface Quality Evaluation Using FESEM and Non-Contact Optical Profilometer

In the present investigation, we carried out FESEM analysis to exemplify the features on the machined surfaces for varying servo settings. Figure 10(a) depicts the morphology of machined surfaces procured at  $SV = 30 \text{ V}$ , and  $SF = 2150 \text{ mm/min}$ . It is noted that the machined surface has microcrack and deep craters which corroborates the uncovering of the surface to high intensified sparks. It is also noted that the machining time is lower, and the perturbations from the actual geometric profile are substantial in this setting as reported in Sect. 3.2, which further endorses that the surface is exposed to high intensified sparks. On the contrary, the surface texture at settings of  $SV = 60 \text{ V}$ , and  $SF = 2150 \text{ mm/min}$  reveals shallow craters illustrating the exposure to low intensified sparks (Fig. 10(b)), which can be further corroborated by the higher machining time and lower geometrical perturbations. It is further intended to assess the topography of machined surfaces at two settings, i.e., at  $SV = 30 \text{ V}$ , and  $SF = 2150 \text{ mm/min}$ , and at  $SV = 60 \text{ V}$ , and  $SF = 2150 \text{ mm/min}$  using a non-contact optical profilometer. The  $R_a$  values are acquired using the 3-D analysis software TalyMap. Figure 11(a) depicts the surface topography of machined surfaces procured at  $SV = 30 \text{ V}$ , and  $SF = 2150 \text{ mm/min}$ , whereas Fig. 11(b) depicts the surface topography of machined surfaces procured at  $SV = 60 \text{ V}$ , and  $SF = 2150 \text{ mm/min}$ . The high density of melted deposits and deep craters, as evident in Fig. 11(a), results in a high surface roughness value of  $2.54 \text{ μm}$  at  $SV = 30 \text{ V}$  and  $SF = 2150 \text{ mm/min}$ . This may be attributed to exposure of the machined surface to a high number of intensified sparks as the inter-electrode gap in such a setting is narrower. The low density of melted deposits and shallow craters, as evident in Fig. 11(b), results in a low surface roughness value of  $1.81 \text{ μm}$  at  $SV = 60 \text{ V}$  and  $SF = 2150 \text{ mm/min}$ . This may be attributed to exposure of the machined surface to a low number of intensified sparks as the inter-electrode gap in such a setting is wider.

## 6 Conclusions

Wire lag is the phenomenon in WEDM that causes inaccuracy in intricate profiles. Previous research endeavors focused on

**Fig. 11** Surface topography using non-contact optical profilometry  
**a** SV = 60 V, SF = 2150 mm/min, **b** SV = 30 V, SF = 2150 mm/min



the effect of common process variables such as pulse duration time ( $P_{on}$ ), pulse width interval ( $P_{off}$ ), and peak current ( $I_p$ ) on the accuracy of complicated profiles in WEDM. The impact of servo feed rate under various control modes on the machining time and accuracy of intricate profiles, on the other hand, was rarely investigated. To accomplish this goal, it is therefore investigated to observe the effects of servo feed rate (SF) and other factors such as the dielectric water pressure (WP), wire tension (WT), and servo voltage (SV) on the three performance qualities. The responses evaluated in this study include machining time (MT), corner error (CE), and radius of the concave profile (RUC). Face-centered central composite design was exploited to plan the experiments. ANOVA test for MT and RUC discloses that SV and SF were the most significant parameters ( $p$  values less than 0.05). Whereas ANOVA test for CE exposes that all the four process parameters were statistically significant. ( $p$  values for the parameters are less than 0.05.) Important interaction effects of the process parameters on the responses were portrayed with the help of contour plots. To optimize the multiple performances simultaneously, an integrated approach, i.e., desirability function with Nelder-simplex algorithm, was proposed in this investigation. The parametric settings recommended by the proposed approach were WP = 15 kg/cm<sup>2</sup>, WT = 12 N, SV = 60 V, and SF = 2150 mm/min and the optimal responses as follows: MT = 31.54 min, RUC = 1.97  $\mu$ m, and CE = 111.43  $\mu$ m.

**Acknowledgements** This study acknowledges the Govt. of India, Ministry of Human Resource and Development for providing scholarship during the research period.

## Declarations

**Conflict of interest** The authors declare that they have no known competing financial interests or personal relationships that could have appeared to influence the work reported in this paper.

## References

1. Dekeyser, W. L.: Geometrical accuracy of wire-EDM. Proc. of ISEM-9, 226–232 (1989)
2. Dauw, D.F.; Beltrami, I.: High-precision wire-EDM by online wire positioning control. CIRP Ann. **43**, 193–197 (1994)
3. Hsue, W.J.; Liao, Y.S.; Lu, S.S.: Fundamental geometry analysis of wire electrical discharge machining in corner cutting. Int. J. Mach. Tools Manuf. **39**, 651–667 (1999)
4. Lin, C.T.; Chung, I.F.; Huang, S.Y.: Improvement of machining accuracy by fuzzy logic at corner parts for wire-EDM. Fuzzy Sets Syst. **122**(3), 499–511 (2001)
5. Puri, A.B.; Bhattacharyya, B.: An analysis and optimisation of the geometrical inaccuracy due to wire lag phenomenon in WEDM. Int. J. Mach. Tools Manuf. **43**, 151–159 (2003)
6. Sarkar, S.; Sekh, M.; Mitra, S.; Bhattacharyya, B.: A novel method of determination of wire lag for enhanced profile accuracy in WEDM. Precis. Eng. **35**, 339–347 (2011)
7. Selvakumar, G.; Sarkar, S.; Mitra, S.: Experimental investigation on die corner accuracy for wire electrical discharge machining of Monel 400 alloy. Proc Inst Mech Eng B J Eng Manuf. **226**, 1694–1704 (2012)
8. Selvakumar, G.; Jiju, K.B.; Sarkar, S.; Mitra, S.: Enhancing die corner accuracy through trim cut in WEDM. Int. J. Adv. Manuf. **83**, 791–803 (2016)
9. Kumar, A.; Kumar, V.; Kumar, J.: Multi-response optimization of process parameters based on response surface methodology for pure titanium using WEDM process. Int. J. Adv. Manuf. **68**, 2645–2668 (2013)
10. Sonawane, S.A.; Kulkarni, M.L.: Multi-feature optimization of WEDM for Ti-6Al-4V by applying a hybrid approach of utility theory integrated with the principal component analysis. Int J Mater Form Mach Processes (IJMFMP) **5**, 32–51 (2018)
11. AbyarFirouzabadi, H.; Parvizian, J.; Abdullah, A.: Improving accuracy of curved corners in wire EDM successive cutting. Int. J. Adv. Manuf. **76**, 447–459 (2015)
12. Yan, M.T.; Huang, P.H.: Accuracy improvement of wire-EDM by real-time wire tension control. Int. J. Mach. Tools Manuf. **44**, 807–814 (2004)
13. Sanchez, J.A.; López de Lacalle, L.N.; Lamikiz, A.: A computer-aided system for the optimization of the accuracy of the wire electro-discharge machining process. Int. J. Comput. Integr. Manuf. **17**(5), 413–420 (2004)
14. Sanchez, J.A.; Rodil, J.L.; Herrero, A.; De Lacalle, L.L.; Lamikiz, A.: On the influence of cutting speed limitation on the accuracy of wire-EDM corner-cutting. J. Mater. Process. Technol. **182**, 574–579 (2007)





15. Werner, A.: Method for enhanced accuracy in machining curvilinear profiles on wire-cut electrical discharge machines. *Precis. Eng.* **44**, 75–80 (2016)
16. Conde, A.; Sanchez, J.A.; Plaza, S.; Ramos, J.M.: On the influence of wire-lag on the WEDM of low-radius free-form geometries. *Procedia CIRP.* **42**, 274–279 (2016)
17. Chen, Z.; Zhang, Y.; Zhang, G.; Li, W.: Modeling and reducing workpiece corner error due to wire deflection in WEDM rough corner-cutting. *J Manuf Process.* **36**, 557–564 (2018)
18. Chen, Z.; Huang, Y.; Zhang, Z.; Li, H.; Yi Ming, W.; Zhang, G.: An analysis and optimization of the geometrical inaccuracy in WEDM rough corner cutting. *Int. J. Adv. Manuf.* **74**, 917–929 (2014)
19. Abyar, H.; Abdullah, A.; Akbarzadeh, A.: Analyzing wire deflection errors of WEDM process on small arced corners. *J Manuf Process.* **36**, 216–223 (2018)
20. Kirwin, R.M.; Moller, J.C.; Jahan, M.P.: Modification and adaptation of wire lag model based on surface feed for improving accuracy in wire EDM of Ti-6Al-4V alloy. *Int. J. Adv. Manuf.* **117**, 2909–2920 (2021)
21. Chakraborty, S.; Bose, D.: Improvement of die corner inaccuracy of inconel 718 alloy using entropy based GRA in WEDM process. *Adv Eng Forum.* **20**, 29–41 (2017)
22. Bisaria, H.; Shandilya, P.: Processing of curved profiles on Ni-rich Nickel–titanium shape memory alloy by WEDM. *Mater. Manuf. Process.* **34**, 1333–1341 (2019)
23. Naveed, R.; Mufti, N.A.; Mughal, M.P.; Saleem, M.Q.; Ahmed, N.: Machining of curved profiles on tungsten carbide-cobalt composite using wire electric discharge process. *Int. J. Adv. Manuf.* **93**, 1367–1378 (2017)
24. Selvakumar, G.; ThiruppathiKuttalingam, K.G.; Ram Prakash, S.: Investigation on machining and surface characteristics of AA5083 for cryogenic applications by adopting trim cut in WEDM. *J. Braz. Soc. Mech. Sci. Eng.* **40**, 1–8 (2018)
25. Yan, H.; Bakadiasa, K.D.; Chen, Z.; Yan, Z.; Zhou, H.; Han, F.: Attainment of high corner accuracy for thin-walled sharp-corner part by WEDM based on magnetic field-assisted method and parameter optimization. *Int. J. Adv. Manuf.* **106**, 4845–4857 (2020)
26. Mandal, K.; Sarkar, S.; Mitra, S.; Bose, D.: Parametric analysis and GRA approach in WEDM of Al 7075 alloy. *Mater. Today: Proc.* **26**, 660–664 (2020)
27. Saha, S.; Maity, S.R.; Dey, S.; Dutta, S.: Modeling and combined application of MOEA/D and TOPSIS to optimize WEDM performances of A286 superalloy. *Soft Comput.* **25**, 14697–14713 (2021)
28. Mustafa, A.H.; Hashmi, M.S.; Yilbas, B.S.; Sunar, M.: Investigation into thermal stresses in gas turbine transition-piece: Influence of material properties on stress levels. *J. Mater. Process. Tech.* **201**, 369–373 (2008)
29. Rao, M.N.: High performance stainless steels for critical engineering applications. *Trans. Indian Inst. Met.* **63**, 321–330 (2010)
30. Derringer, G.; Suich, R.: Simultaneous optimization of several response variables. *J. Qual. Technol.* **12**, 214–219 (1980)
31. Mobin, M.; Mousavi, S.M.; Komaki, M.; Tavana, M.: A hybrid desirability function approach for tuning parameters in evolutionary optimization algorithms. *Measurement* **114**, 417–427 (2018)
32. Chabbi, A.; Yallese, M.A.; Meddour, I.; Nouioua, M.; Mabrouki, T.; Girardin, F.: Predictive modeling and multi-response optimization of technological parameters in turning of Polyoxymethylene polymer (POM C) using RSM and desirability function. *Measurement* **95**, 99–115 (2017)
33. Chen, Z.; Wu, L.; Lin, P.; Wu, Y.; Cheng, S.: Parameters identification of photovoltaic models using hybrid adaptive Nelder-Mead simplex algorithm based on eagle strategy. *Appl. Energy.* **182**, 47–57 (2016)
34. Brabender, S.; Kallis, K.T.; Keller, L.O.; Poloczec, R.R.; Fiedler, H.L.: Optimization of reactive ion etching processes using desirability. *Microelectron. Eng.* **87**, 1413–1415 (2010)

